Microelectronic Engineering 193 (2018) 13–17

Contents lists available at ScienceDirect

Microelectronic Engineering

journal homepage: www.elsevier.com/locate/mee

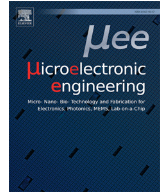

Impact of sub- and supra- threshold switching in the synaptic behavior of TiO_2 memristors

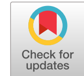

N. Ghenzi [a,b,*], P. Levy [a,b,c]

[a] GIANN, CNEA; San Martín, Buenos Aires, Argentina
[b] CONICET, Argentina
[c] ECyT, UNSAM, Argentina

A R T I C L E   I N F O

Article history:
Received 11 July 2017
Received in revised form 10 February 2018
Accepted 17 February 2018
Available online 20 February 2018

Keywords:
Oxide
Memristor
Resistive switching
Memory

A B S T R A C T

Al/TiO_2/Au memory junctions grown by reactive sputtering were fabricated and characterized. Usual hysteretic features were obtained, spanning an order of magnitude ratio between high and low resistance states. We explored sub-threshold and supra-threshold stimuli, to describe "binary" and "analogic" synapses (i.e. synaptic emulators) characteristics in detail. We show that each type of behavior can be chosen regarding the dependence of the switching on the amplitude of voltage stimuli. The sub-threshold switching originating the analog mode is explained by the drift-diffusion of oxygen vacancies while the binary mode is attributed to the Joule-heating-assisted electric-field-induced movement of oxygen vacancies. In the supra-threshold limit we found that "excitatory" and "inhibitory" synaptic behavior can be tailored by controlling the pulsing current amplitude. We discuss this result within the artificial neural network topology framework, as changing the behavior type of the synapses results in its reconfiguration.

© 2018 Elsevier B.V. All rights reserved.

1. Introduction

Electrical resistance switching (RS) between high (HRS) and low (LRS) resistance states seems to be ubiquitous in metal-oxide interfaces [1]. The non-volatile character of these reversibly switchable remnant resistance states envisages their practical use for low power massive storage media, i.e. portable memory devices. Resistive random access memories (ReRAMs, also called memristors) based on the RS phenomena are usually formed by a simple capacitor-like geometry (typically a metal-insulator-metal MIM structure) and depict high switching speed and downscaling possibilities, already demonstrated down to the nanoscale [2].

Besides, ReRAM devices depict multilevel capability [3]. Intermediate resistance states lying between HRS and LRS "digital" states give rise to the so called "analogical" memories [4], exhibiting synaptic-like capabilities. Usually the existence of a well-defined threshold stimulus for the writing operation allows performing un-disturbing measurements of remnant resistance values [5].

By injecting a stimulus close to but below this threshold a "sub-threshold" memristor can be implemented, which is useful because of its analog properties. The sub- and supra-threshold switching is related to the local-temperature-induced enhancement of the oxygen vacancies drift-diffusion [6]. A proper understanding of the sub-threshold switching is lacking to validate their use in analog circuits. Indeed, more and more electronic designers concentrate their research on the development of neuromorphic systems implemented with circuits and devices operating in the sub-threshold domain [7].

Recently, the possibilities and advantages of using the synaptic behavior of memristors in artificial neural networks (ANN) to fabricate computers with features emulating the human brain have been analyzed [8]. We envisage that tuning the combined drift and diffusion mechanisms and controlling its amplitude through the local temperature can affect and control the synaptic properties of memristors. Specifically, here we suggest the possibility to use the sub- and supra-threshold behavior of the resistance in ReRAM devices in order to drive their analog/digital, and excitatory/inhibitory synaptic modes in TiO_2 junctions. These findings will decrease the complexity of ANN because analog and digital circuits could be integrated in the same place of a neuromorphic chip. Our results fill the gap in the architecture of neuromorphic systems allowing ANN to evolve to reconfigurable structures [9] likewise biological systems.

2. Methods

We study Al(100 nm)/TiO_2(50 nm)/Au(50 nm) junctions of 10 um × 10 um area in a crossbar pattern as shown in the SEM image of Fig. 1(a). The device was cut with a FIB previous to the SEM image. Amorphous TiO_2 films were deposited by reactive sputtering with a pressure of 20 mTorr, and a power of 150 W at room temperature.

* Corresponding author at: GIANN, CNEA; San Martín, Buenos Aires, Argentina.
E-mail address: n.ghenzi@gmail.com (N. Ghenzi).

https://doi.org/10.1016/j.mee.2018.02.017
0167-9317/© 2018 Elsevier B.V. All rights reserved.

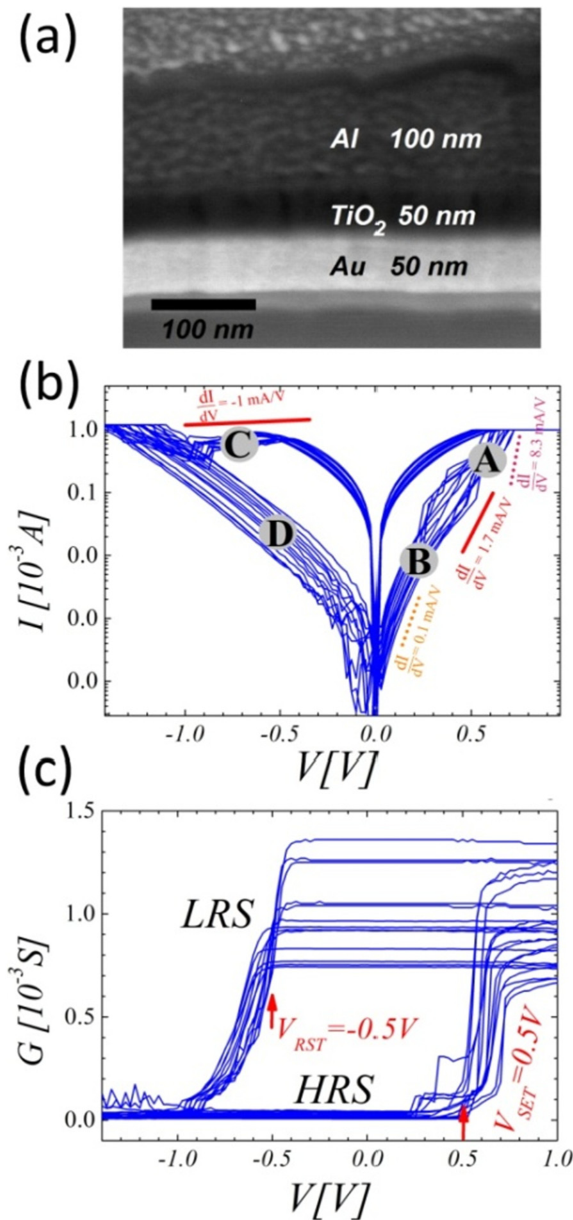

Fig. 1. (a) Cross-section SEM image of the MIM structure. The cross section was cut with an FIB and tilted 45° to be observed with the SEM. (b) I-V response of Al/TiO_2/Au junction. Different dI/dV regimes are depicted. (c) Non-volatile response (read current/0.1 V) showing the low (LRS) and high resistance (HRS) states in conductance units. The threshold voltages are +0.5 V for the SET process and −0.5 V for the RST process.

The two metals acting as bottom (BE: Au) and top (TE:Al) electrodes were deposited by DC sputtering in an Argon atmosphere. To get the crossbar pattern we employ a lift off process to define each one of the three layers of the junction (TE = Al, TiO_2 and BE = Au) [10]. The electrical characterization (I-V curves) was performed with a source-measurement unit Keithley 2400, with the BE grounded.

3. Results and discussion

We start by forming the device with a DC voltage sweep up to 15 V, with 1 mA current limit (data not shown). After this initial process the device exhibits reversible RS. To characterize the switching effect we follow by measuring the electrical response of the Al/TiO_2/Au junctions. We choose a pulsed I-V protocol with a voltage width pulse of 10 ms and a time between voltages pulses of 250 ms. In order to avoid hard breakdown of the titanium dioxide we set a compliance value of 1 mA. Using these conditions the RS phenomena is observed, exhibiting two (digital) stable states, namely the HRS and LRS states depicted by two branches of the I-V curve, see Fig. 1(b). We also measure the remnant conductance (@ 0.1 V) between voltage pulses to characterize the non-volatile response, as shown in Fig. 1(c).

The main feature of our RS devices is the hysteresis of the current-voltage (I-V) loop presented in Fig. 1(b). Two different branches are observed, corresponding to HRS and LRS states. The transition from HRS to LRS, or SET, occurs when the voltage exceeds $V^{+}_{th} \sim +0.5$ V. Reset transition or RST, is observed at negative $V < V^{-}_{th} \sim -0.5$ V. The low bias resistance ratio (r) exceed one order of magnitude, defined as the ratio between the HRS = 12 kΩ and the LRS = 1 kΩ, i.e. $r \sim 12$.

During the rapid transition from HRS to LRS the device traverses a multitude of different resistance states which can be defined as a new LRS if the voltage sweep is stopped. This feature is a clear signature of the memristive properties of the interface. Eventually the minimum LRS resistance value = 850 Ω is reached at the maximum positive polarity pulsing, and it remains stable through the rest of the loop. It is noteworthy to mention that the HRS value is unaltered during several cycles, while the LRS changes between 850 Ω and 1.2 kΩ, see Fig. 1(c), where for clarity we depict resistance values in conductance units.

This bipolar RS behavior (RST and SET occur at opposite polarity) is a strong signature of the physical underlying mechanism. First of all, during the electroforming step, an oxygen vacancy filament is originated at the TiO_2 film. The oxygen vacancy filament mimics a local non-stoichiometric oxide phase that contains OV in higher densities closer to the TE interface. Additionally, and taking into account that the Al/TiO_2 interface is ohmic, the oxygen vacancies located near the tip of the filament at the Au/TiO_2 interface are drifted back and forth. The density of the remaining oxygen vacancies determines the resistance of the device. In this way, this resistive device acts as a monitor of oxygen vacancies near the tip of the filament at the Au/TiO_2 interface. We reported a comprehensive analysis of our resistive switching devices in a previous publication [10].

By tailoring the nature of the sample, it is expected that we can induce additional states by manipulating the oxygen vacancy density at the tip of the filament in the active metal-oxide interface (i.e. the device response function evolves from a binary logic to an analog one). It was already proven that the multilevel characteristics of TiO_2-based RS can be reliably tuned by adjusting the defect characteristics [11] tailoring the deposition conditions. Additionally, considering that the LRS has the highest density of oxygen vacancies at the tip of the filament in the Au/TiO_2 interface, we can relate its variability to the movable oxygen ions available at the Au electrode [10].

In ref. [12], the authors studied the analog switching in order to obtain intermediate states. An alternative way to study the transition from binary to analog switching is through the fine tuning of the stimuli. In the following we explore the threshold strength for inducing the RS phenomena. The threshold stimulus V_{th} is the weakest stimulus that could generate a RS effect at the TiO_2 junction. From a microscopic point of view, it is related to the energy barrier to move an oxygen ion from one site of the lattice to another. From a practical point of view, this implies that, if a voltage sweep is applied reaching a voltage value below the threshold value, then no hysteresis is observed. Contrarily, if the maximum amplitude of the voltage sweep is higher than the threshold value, the I-V exhibits hysteresis.

We select different ranges at the I-V curve to define *supra* and *sub -threshold* conditions. The ranges A and C in Fig. 1(b) are regions where voltage pulses belong to the *supra-threshold* condition of positive and negative polarities, respectively. On the other hand, B and D regions are *sub-threshold* voltage pulses for the positive and negative polarities, respectively.

Initially we choose *voltage* as the stimuli to perform the analysis. In Fig. 2(a) we apply 100 positive *voltage* pulses of +0.7 V amplitude (supra-threshold condition, A range, blue squares). We obtain an *abrupt* increase in the conductance after applying the very 1st

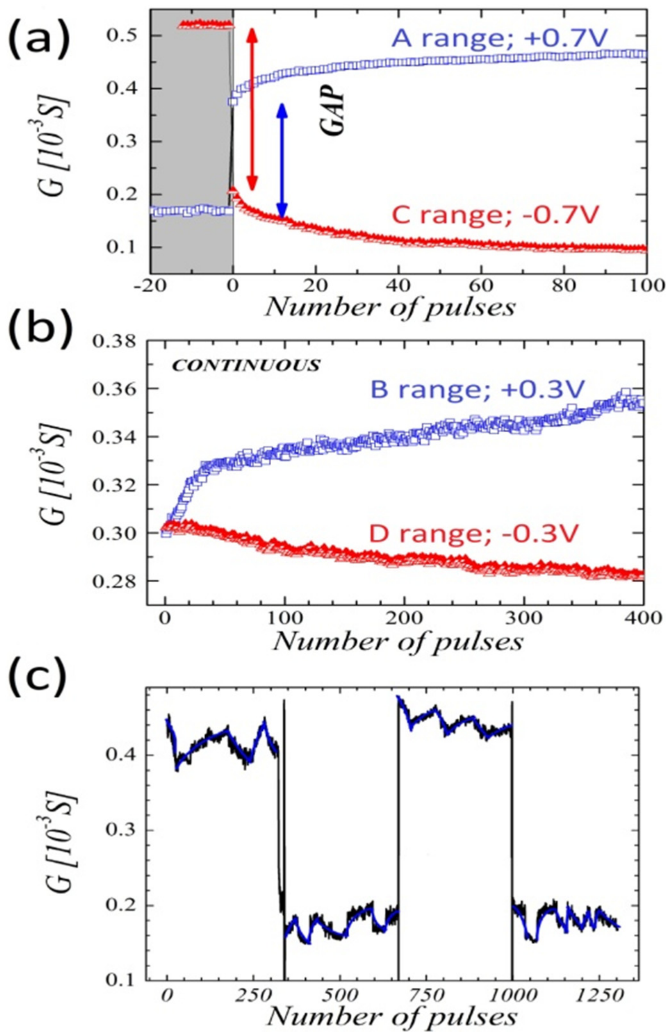

Fig. 2. Conductance response showing the analog and digital characteristics of Al/TiO_2/Au junctions. (a) Conductance response to initial 100 pulses with +0.7 V (blue squares) and −0.7 V (red triangles), both in the supra-threshold condition. (b) Conductance response to initial 400 pulses with +0.3 V (blue squares) and −0.3 V (red triangles), both belong to sub-threshold condition. (c) Modulation of the conductance of the TiO_2 junction with ±0.3 V (sub-threshold condition) with exception of pulses #350, #675 and #1000 where we switch the device between the LRS and HRS states with *single* ±0.7 V pulses. This experiment shows the simultaneous targeting of sub and supra threshold resistive switching. It is important to note that in the digital mode we obtained eight times the change in conductance compared to the change in the analog mode with one quarter of the total number of pulses. (For interpretation of the references to color in this figure legend, the reader is referred to the web version of this article.)

pulse, accounting for most (~80%) of the total change (the remaining 20% increase is attained after the application of the ulterior 99 pulses).

Using negative polarity, and starting from this LRS state, we apply 100 voltage supra-threshold −0.7 V pulses at the C range (a much lower current flows in the negative case, as compared to the positive one, due to the rectifying properties of the Schottky barrier at the Au/TiO_2 interface). We again observe a gap or *abrupt* change after the first pulse, but with decreasing conductance values, as shown in Fig. 2(a) in red triangles. Interestingly, for both A- and C-ranges, as we continue applying voltage pulses after the 1st voltage pulse, the change is smooth, monotonic and continuous, accounting for a ~20% change. After 100 pulses the ratio between the initial and final conductance values was 2.7 (A range) and 5 (C range). In brief, switching with supra-threshold voltage pulse type can be classified as a “digital” mode accounting for 80% change of the initial value, with an ulterior smooth tendency towards saturation.

Now we proceed to describe the results with sub-threshold voltage pulses. In Fig. 2(b) we apply 400 voltage pulses of +0.3 V and −0.3 V respectively. In the B range (+0.3 V, blue squares) we observe a continuous increase of the conductance with a total amplitude change of 1.2 times. In the D range (the sub-threshold condition in negative polarity), we observe a continuous decrease of the conductance value (−0.3 V, red triangles) accounting a total amplitude change of ~1.1 times. In these cases (B and D ranges) the switching with sub-threshold pulses type can be classified as an “analog” mode with an overall change of <10% after applying the initial 100 pulses.

Measurements depicted in Fig. 2(a) and (b) allow classifying the RS response as either “digital” or “analog” switches respectively. Quantitatively, 200–500% changes are observed in the supra-threshold regime, while the sub-threshold one can only account for a 10% change. From a practical point of view they indicate that a certain conductance value can be tuned to whichever desired value between the HRS and LRS extreme values by applying a proper combination of sub and supra threshold voltage pulses. The way in which a given conductance value can be obtained changes in accordance to the voltage amplitude of the applied pulses. Namely, we can switch between two conductance states with only one pulse in an abrupt way (supra-threshold condition of the pulses) or with many pulses in a continuous (or smooth) way (sub-threshold pulsing).

With the purpose of testing the combined modulation of conductance in both extreme conductance states (LRS and HRS) we performed the experiment depicted in Fig. 2(c). We show the conductance of the device (read current/0.1 V) as a function of the number of pulses Np. We set the device at HRS, LRS and HRS states in pulses number #350, #675 and #1000 respectively. This means that for Np in the ranges (0:350) and (675:1000) the device is in LRS state, and for Np in the ranges (350:675) and (1000:1300) the device is in the HRS state. As it is evident, these three transitions were realized with voltage pulses in the supra-threshold condition. Now we proceed to focus on the effect of voltage pulses in the sub-threshold condition. Firstly we chose the LRS in the (0:350) range. In this case we only apply pulses of ±0.3 V and we can modulate the conductance 0.04 ms around 0.42 ms in an arbitrary way. In a similar way, in the HRS obtained for Np between (350:675) we can again modulate the conductance with pulses of ± 0.3 V but now the conductance is modulated 0.02 ms around 0.18 ms. The same behavior is observed for the LRS with Np in the (675:1000) range and for the HRS with Np in the (1000:1300) range.

Thus, both regimes coexist in a single device. This fact can be used to integrate both analog and digital responses in the same physical location, reducing circuit complexity with the added capacity of switching between both modes, thus resulting in a mixed digital and analog reconfigurable circuit.

Typically the monotonous and continuous increase and decrease of the resistance due to the accumulation of pulses has been related to the depression and enhancement of the synaptic weight in neural networks [13]. Furthermore, in Reference [14] the authors used this property to show that the SET transition of an oxide synaptic device becomes probabilistic with sub-threshold pulses, while in our case the RS is continuous and deterministic. The appearance of the probabilistic or deterministic switching is related to the time width of the pulses: for very short pulses the probabilistic behavior appears, while long pulses produces deterministic behavior. These two types of switching are the demonstration of the same phenomena, namely the RS due to the drift-diffusion of oxygen vacancies without a noticeable thermal assistance. This property was already used to demonstrate a 100 times decrease in the energy consumption when training large-scale deep networks [15].

A signature to clarify the underlying mechanism is related to the conductance change rate with respect to Np. From Fig. 2(c) we can infer that the switching in one voltage pulse of the same time width is 3000 times higher in the supra-threshold condition than in the sub-threshold one (0.02 ms of conductance change with 300 pulses vs

0.2 ms with one pulse respectively). This exponential increase of the conductance change rate is related to the electric field enhanced drift of oxygen vacancies in combination with thermal assistance [16]. This increase in the defect kinetics activated by the local temperature in the narrowest region of the filament (the filament tip at the Au/TiO_2 interface) enables an improved emulation of the synaptic functionality and it complements other similar alternatives like ionic drift [17], thermal dissipation [18], mobility decay [19] or nanoparticle diffusion [16]. It is noteworthy to mention that the *drift and diffusion kinetics* define the performance specifications of memristive devices such as switching speed, retention time and overall endurance.

The supra-threshold response was further explored in detail by means of current driven stimulus. When the SET transition is driven by the voltage as stimuli, the sudden change from HRS to LRS produces an uncontrolled peak of power at the resistive device. Power dissipated in this process determines the local temperature inside the oxide and therefore controls the drift-diffusion of the oxygen vacancies. As the power dissipation can be self-limited by applying electrical current as the stimulus [21], we next used current pulses to explore different regions of the I-V curve, labeled by their dI/dV response, as depicted in Fig.1(b).

Note the very different response according to the current amplitude in Fig. 1(b). Let's analyze the derivative *dI/dV* in the first quadrant of the I-V response (range related to the SET process). For pulses below 50 μA, *dI/dV* ~ 0.1 mA/V, and we expect to be in the deep sub-threshold range. For pulses ranging between 50 μA and 0.5 mA, *dI/dV* ~ 1.7 mA/V, while in the 0.5 mA–1.0 mA range, *dI/dV* ~ 8.3 mA/V. On the other hand, in the third quadrant related to the RST process, *dI/dV* is −1 mA/V for pulses between −0.5 V and −1 V (we only considered this range due to the region where the RST process is in the supra-threshold condition). This very different behavior indicates that pulsing with current values will determine a better control of the synaptic properties [21]. We chose +0.4, 0.5, 0.8 and 0.9 mA that have very different *dI/dV* values. Note that this range of current stimulus corresponds to the +0.5 V range stimulus.

We show the results with the selected current pulses in Fig. 3, with the conductance (read current/0.1 V) as a function of the number of pulses. For proper comparison we always set the device (Fig. 3) at the same conductance initial state (50 μs). When pulsing with Ip < 0.5 mA the first pulse switches abruptly the device, and after it continues increasing the conductance value in a smooth way [22]. Following our previous labeling, they are in the "A" region. After, we apply a 100 negative current polarity with the same current amplitude. These 100 pulses produce the same smooth switching behavior than the first 99 positive current pulses, though with decreasing conductance values.

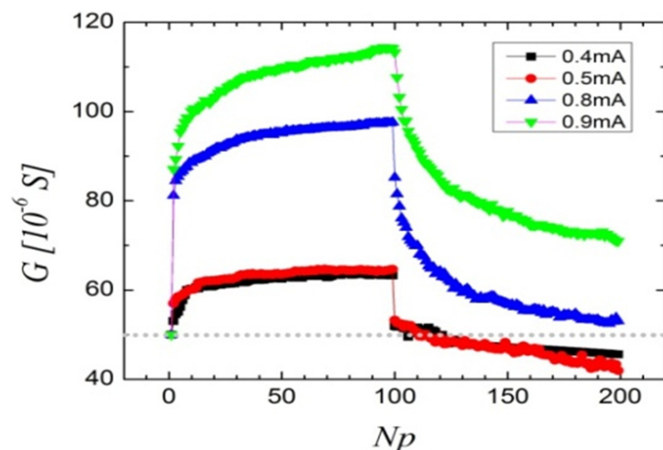

Fig. 3. Excitatory and inhibitory synaptic behavior. The mode can be chosen in accordance to the current amplitude of the stimuli, getting advantage of the different dI/dV in the I-V response. Set and Reset processes are obtained with same amplitude current pulse and opposite polarity.

As shown in Fig. 3, although the change produced by a set of current pulses is drastically reduced as compared to that produced by the same amount of voltage pulses, qualitative features remain similar. It is important to mention that for −0.4 mA and −0.5 mA the conductance jump after the first 100 positive current pulses is higher than that for −0.8 mA and −0.9 mA. This is related to the actual conductance state for Np = 100: when the conductance is smaller, the electric field moving the oxygen vacancies will be higher, thus generating a higher conductance jump.

In the 4 cases we obtained the same potentiation (positive pulses) and depression (negative) –like exponential behavior of the conductance [23]. Nevertheless, the overall difference comes from the conductance constant change after the whole cycle. For the 0.4 and 0.5 mA pulses case the increase in the conductance in the first 100 + pulses is lower than the decrease in the last 100 – pulses determining a final conductance state which is *lower* than the initial one. On the other hand, with 0.8 and 0.9 mA pulses the increase in the conductance in the first 100 + pulses overcomes the decrease in the last 100 – pulses, resulting in a *higher* conductance state, as compared to the initial one.

Usually, excitatory and inhibitory biological synapses [20] play a crucial role in the cortical activity of the brain. With the aim to control the appearance of these modes we analyze the conductance behavior. In our artificial synapses, the difference in the final conductance state compared to the initial one is related to the different *dI/dV* in the SET process (1.7 mA/V corresponding to 0.4 and 0.5 mA pulses compared to 8.3 mA/V corresponding to 0.8 and 0.9 mA pulses). We can ascribe this difference to the behavior of excitatory and inhibitory synapses.

In Ref. [24] the same effect of potentiation and depression is done by varying the pulse time width on PCMO based-memristors. In their model, the authors ignored the fact that initial and final conductance state are different (this fact can be seen in Fig. 3 and it is not reproduced in Fig. 8 of ref. [24]). The difference between initial and final states is related to the asymmetrical electric field profile inside the oxide originating the back and forth oxygen vacancies movement. A detailed discussion can be found in ref. [10] and references therein.

To fabricate an analog ANN the circuit element for the synapses is extremely important, because the number of synapses is much larger than that of neurons. Additionally, artificial neurons are built of many complex transistors while synapses are made by only one simple MIM structure. Therefore, memristor synapses increase noticeably the quantity of synapses that can be fabricated in a given ANN. More important, the change from excitatory to inhibitory neurons has to be done rewiring its transistors [25], while here we show that the same change in memristor synapses can be done by simply adjusting current pulse amplitude (i.e. the stimuli). Note this is similar to biological neural networks, where excitatory and inhibitory synapses are defined by its neurotransmitter [25].

4. Conclusions

We showed that Al/TiO_2/Au memory junctions can emulate "binary" and "analogic" synapses by controlling the voltage pulse amplitude. Both types of synapses can coexist in the same device when changing the amplitude of the stimuli. The sub-threshold switching is then explained by the drift-diffusion of oxygen vacancies with local thermal assistance inside the amorphous structure of titanium dioxide. We found that controlling the amplitude of the current stimuli, a simultaneous "excitatory" and "inhibitory" synaptic behavior appears. Besides, in contrast to the voltage controlled mode, the resistive switching amplitude is controlled by the initial conductance value. As changing the behavior type of the synapses results in the reconfiguration of the ANN topology, above described results could be implemented in a new ANN generation with improved capabilities.

Acknowledgments

We acknowledge the SEM/FIB images to Gustavo Giménez at CMNB - INTI, and financial support from PIP 2015–2017 #322.

References

[1] R. Waser, R. Dittmann, G. Staikov, K. Szot, Adv. Mater. 21 (2009) 2632.
[2] M. Rozenberg, Scholarpedia 6 (2011), 11414. .
[3] P. Stoliar, et al., IEEE Trans. Circuits Syst. II, Analog Digit. Signal Process. 61 (21) (2014).
[4] J.J. Yang, et al., MRS Bull. 37 (2012) 131.
[5] D. Colliaux, P. Yger, K. Kaneko, J. Comput. Neurosci. 39 (255) (2015)https://doi.org/10.1007/s10827-015-0575-3.
[6] N. Ghenzi, et al., Appl. Phys. Lett. 104 (2014), 183505. .
[7] A. Roy, P.J. Grossmann, S.A. Vitale, B.H. Calhoun, 17th IEEE International Symposium on Quality Electronic Design (ISQED), 2016 158–162.
[8] N. Serafino, M. Zaghloul, IEEE 56th International Midwest Symposium on Circuits and Systems (MWSCAS), Columbus, OH, 2013, 2013 602–603, https://doi.org/10.1109/MWSCAS.2013.6674720.
[9] S.J. Lee, et al., J. Neurosci. 16 (2016) 2768.
[10] N. Ghenzi, M.J. Sánchez, P. Levy, J. Phys. D. Appl. Phys. 46 (2013) 41.
[11] N. Ghenzi, M.J. Rozenberg, R. Llopis, P. Levy, L.E. Hueso, P. Stoliar, Appl. Phys. Lett. 106 (2015), 123509. .
[12] S. Wang, et al., Microelectron. Eng. 168 (2017) 37.
[13] A. Thomas, J. Phys. D. Appl. Phys. 46 (2013), 093001. .
[14] S. Yu, et al., Front. Neurosci. 7 (186) (2013) 10–3389.
[15] S. Eryilmazet, al, IEEE Trans. Electron Devices 63 (2013) 5004.
[16] Z. Wang, et al., Nat. Mater. 16 (2017) 101.
[17] A. Thomas, J. Phys. D. Appl. Phys. 46 (2013), 093001. .
[18] S. Kim, et al., Nano Lett. 15 (2015) 2203–2211.
[19] C. Du, W. Ma, T. Chang, P. Sheridan, W.D. Lu, Adv. Funct. Mater. 25 (2015) 4290.
[20] Y. Cao, et al., Proc. Natl. Acad. Sci. 93 (9844) (1996).
[21] A.J. Lohn, et al., Appl. Phys. Lett. 105 (10) (2014).
[22] S. Brivio, et al., Int. Conf. in memristive systems, Gradual Set Dynamics in HfO_2-based Memristor Driven by Sub-threshold Voltage Pulses, 2015.
[23] M. Migliore, G. Simone, R. Migliore, Biophys. J. 108 (2015) 1038.
[24] J.W. Jang, et al., IEEE International Symposium on Circuits and Systems, ISCAS, 2014https://doi.org/10.1109/ISCAS.2014.6865320.
[25] F. Nadim, D. Bucher, Curr. Opin. Neurobiol. 29 (2014) 48.